Published in final edited form as:
Biochim Biophys Acta. 2010 ; 1802(7-8): 659–672. doi:10.1016/j.bbadis.2010.04.002.

Muscle Degeneration in Neuramindase 1 Deficient Mice Results from Infiltration of the Muscle Fibers by Expanded Connective Tissue

Edmar Zanoteli[a], **Diantha van de Vlekkert**[a], **Erik J. Bonten**[a], **Huimin Hu**[a], **Linda Mann**[b], **Elida M. Gomero**[a], **A. John Harris**[c], **Giulio Ghersi**[d], and **Alessandra d'Azzo**[a,*]

[a] Department of Genetics, St. Jude Children's Research Hospital, 262 Danny Thomas Place, Memphis, TN 38105, USA [b] Cell & Tissue Imaging Center, St. Jude Children's Research Hospital, 262 Danny Thomas Place, Memphis, TN 38105, USA [c] Department of Physiology, University of Otago, Dunedin, New Zealand [d] Dipartimento di Biologia Cellulare e dello Sviluppo, Università di Palermo, Italy

SUMMARY

Neuraminidase 1 (NEU1) regulates the catabolism of sialoglycoconjugates in lysosomes. Congenital NEU1 deficiency in children is the basis of sialidosis, a severe neurosomatic disorder in which patients experience a broad spectrum of clinical manifestations varying in the age of onset and severity. Osteoskeletal deformities and muscle hypotonia have been described in patients with sialidosis. Here we present the first comprehensive analysis of the skeletal muscle pathology associated with loss of Neu1 function in mice. In this animal model, skeletal muscles showed an expansion of the epimysial and perimysial spaces, associated with proliferation of fibroblast-like cells and abnormal deposition of collagens. Muscle fibers located adjacent to the expanded connective tissue underwent extensive invagination of their sarcolemma, which resulted in the infiltration of the fibers by fibroblast-like cells and extracellular matrix, and in their progressive cytosolic fragmentation. Both the expanded connective tissue and the juxtaposed infiltrated muscle fibers were strongly positive for lysosomal markers, and displayed increased proteolytic activity of lysosomal cathepsins and metalloproteinases. These combined features could lead to abnormal remodeling of the extracellular matrix that could be responsible for sarcolemmal invagination and progressive muscle fiber degeneration, ultimately resulting in an overt atrophic phenotype. This unique pattern of muscle damage, which has never been described in any myopathy, might explain the neuromuscular manifestations reported in patients with the type II severe form of sialidosis. More broadly, these findings point to a potential role of NEU1 in cell proliferation and extracellular matrix remodeling.

Keywords

NEU1; sialidosis; metalloproteinase; muscle biopsy; lysosomes; ECM

[*]Corresponding author. Tel: +1 901 595 2698; fax: +1 901 595 6035. Sandra.dazzo@stjude.org.
Current address: Edmar Zanoteli, Department of Neurology, University of Sao Paulo, Sao Paulo, Brazil. zanoteli@terra.com.br.

1. INTRODUCTION

Compartmentalized degradation of sialoglycoconjugates is initiated in lysosomes by the glycosidase N-acetyl-α-neuraminidase-1 (NEU1), a pivotal enzyme required for the removal of terminal sialic acid residues [1]. NEU1 is transported to lysosomes and activated therein by associating with the serine carboxypeptidase protective protein/cathepsin A (PPCA) [2]. NEU1 is a component of a multiprotein complex containing PPCA, β-galactosidase, and N-acetylgalactosamine-6-sulfate sulfatase. Two genetically distinct lysosomal storage diseases are associated with NEU1 deficiency: sialidosis, which results from structural mutations at the *NEU1* locus on chromosome 6p21 [3] and galactosialidosis, which is caused by a primary defect of PPCA, leading to secondary deficiencies of NEU1 and β-galactosidase [4]. Patients with sialidosis experience a broad spectrum of clinical manifestations, varying in the timing of onset and severity of the symptoms and mostly correlating with the levels of residual enzyme activity [5]. Type I sialidosis, the attenuated form of the disease, occurs during the second decade of life and results in progressive loss of vision associated with nystagmus, ataxia, and grand-mal seizures but not dysmorphic features [3]. Type II sialidosis, the severe form of the disease, is characterized by hydrops foetalis and neonatal ascites, the presence of abnormal somatic features, and severe neurologic involvement. A subset of patients with sialidosis presents with symptoms of profound muscle dysfunction, including muscle hypotonia, atrophy, and osteoskeletal deformities [5]. However, a detailed characterization of the muscle involvement in these patients has never been reported.

Neu1$^{-/-}$ mice develop a systemic disease that closely mimics the pathologic manifestations seen in patients with the early-onset forms of sialidosis, including growth retardation, splenomegaly, severe neurologic deterioration, and premature death [6]. Spleen enlargement in these mice coincides with the time-dependent occurrence of extramedullary hematopoiesis. Our previous studies of the molecular bases of this phenotype identified Neu1 as a negative regulator of lysosomal exocytosis [7]. The latter is a Ca^{2+}-dependent process that entails the recruitment/docking of lysosomes to the plasma membrane (PM), the fusion of the lysosomal membrane with the PM, and the release of lysosomal contents into the extracellular matrix (ECM) [8]. We found that the lysosomal-associated membrane protein-1 (Lamp-1), which has been implicated in the recruitment/docking of lysosomes to the PM, is a substrate of Neu1. In the absence of Neu1, oversialylated Lamp-1 has a longer half-life, and this increases the number of lysosomes poised to dock at the PM and to engage in lysosomal exocytosis [7]. The downstream effect is the enhanced release of catalytically active proteases and glycosidases extracellularly, a phenomenon that affects the processing of cell surface proteins and ECM components [7]. In the fibroblasts of patients with sialidosis who have different clinical phenotypes, we demonstrated an inverse correlation between the levels of the residual NEU1 activity and the increase in lysosomal exocytosis. Given the ubiquitous tissue distribution of this lysosomal enzyme, it is conceivable that the process of lysosomal exocytosis in absence of Neu1 activity is deregulated in other tissues and underlie many of the pathologic manifestations characteristic of this disease, albeit the downstream effects of this process may be cell-type specific.

In addition to their role in the intralysosomal catabolism of sialylated macromolecules, NEU1 and PPCA are found at the cell surface together with the elastin-binding protein as part of the elastin receptor protein complex [9,10]. It has been postulated that within this complex NEU1 participates in the regulation and assembly of the elastic fibers [9,11]. Recently, Starcher *et al.*, [12] demonstrated that elastic fiber deposition is altered in the aorta and lung of *Neu1*-null mice, and that the impaired extracellular assembly of the elastic fibers causes this effect. In skeletal muscle, the interplay between the ECM and individual muscle fibers is crucial for the normal function and integrity of this tissue. In addition to providing mechanical support, the ECM, and in particular the basement membrane/basal lamina,

function as a scaffold during muscle regeneration. Components of these structures and the muscle fibers, such as collagens, laminins, integrins, and dystroglycans, represent bona fide signaling molecules that play key roles in muscle development, maintenance, and regeneration. Disturbing any of these components may adversely affect muscle strength and integrity and result in muscle disease [13–15]. The concept that NEU1 may directly or indirectly influence the behavior of extracellular components by altering the sialic acid content of intracellular and extracellular substrates could be a common determinant of many of the systemic abnormalities characteristic of sialidosis.

Here we show that in *Neu1*$^{-/-}$ mice, muscle fibers undergo progressive disruption associated with profound alterations of ECM components and infiltration by connective tissue. Many of these abnormalities can be attributed to excessive expansion of perimysial and endomysial connective tissue, coupled to increased proliferation of fibroblast-like cells, abnormal deposition of collagen fibers, and enhanced proteolytic activity in the ECM. These findings explain, in part, the neuromuscular signs and symptoms described in patients with sialidosis and indicate a primary role of NEU1 in the pathogenesis of muscle diseases.

2. MATERIALS AND METHODS

2.1. Animals

Neu1$^{-/-}$ and wild-tye (WT) mice (FVB/NJ background), aged 15 days to 7 mo, were included in this study. The *Neu1*$^{-/-}$ mice were previously generated in our laboratory by targeted disruption in the *Neu1* locus [6]. Animals were housed in a fully AAALAC-accredited animal facility with controlled temperature (22 °C), humidity, and lighting (alternating 12 h light-dark cycles). Food and water were provided *ad libitum*. All procedures in mice were performed according to animal protocols approved by our Institutional Animal Care and Use Committee and NIH guidelines.

2.2. Histology

The *gastrocnemius*, *tibialis anterior*, *quadriceps*, and diaphragm were excised for analysis. The gastrocnemius muscles were weighed for comparison between *Neu1*$^{-/-}$ [1–2 mo (n=6), 3–4 mo (n=5), and 5–6 mo (n=5)] and WT [1–2 mo (n=8), 3–4 mo (n=4), and 5–6 mo (n=5)] mice. The muscle tissues were dissected, frozen immediately in isopentane cooled in liquid nitrogen, and stored at −80 °C until processed for histologic analysis. Fragments of muscle tissues were also fixed in 4% paraformaldehyde (PFA) for immunohistochemical analysis and 4% glutaraldehyde for electron microscopy. Longitudinal or transverse sections (8 μm) of the frozen muscles were cut on a cryostat (Leica CM3050). The sections were stained with hematoxylin and eosin (H&E) for overall morphologic assessment. Cross-sectional areas of *gastrocnemius* muscles from three *Neu1*$^{-/-}$ mice and three matching controls (5–6 mo) stained with H&E were measured by tracing each individual myofiber by using the ImageJ software (NIH Software). At least 200 fibers were measured per animal in three different fields of gastrocnemius muscles.

2.3. Immunohistochemistry

The indirect immunofluorescence method was done for the analyses of the following proteins: transcription factor 4 (TCF4; rabbit monoclonal, Cell Signalling #2565, 1:100), dystrophin (mouse monoclonal, Sigma D8168, 1:400), β-dystroglycan (mouse monoclonal, Abcam ab49515, 1:200), and laminin (rabbit polyclonal, Sigma L9393, 1:200). Frozen sections were blocked with blocking solution containing 2% BSA and 10% normal serum in PBS for 30 min. Sections used for monoclonal antibodies were incubated with AffiniPure Fab Fragment Goat Anti-Mouse IgG (H+L) (Jackson ImmunoResearch) in PBS for 1 hour. Sections were incubated with primary antibodies diluted in blocking solution for at least 1

hour at room temperature or overnight at 4 °C, washed 3 times for 10 min with PBS, and blocked with blocking solution for 10 min. The sections were incubated with Alexa-488 or Cy3 (anti-mouse or anti-rabbit), with or without 488-phalloidin for 40 min, washed in PBS (5 times for 5 min) and mounted with Vectashield mounting medium/DAPI (Vector, H1000). As an internal control, samples were incubated with only the secondary antibody. The slides were examined under a fluorescent microscope (Olympus BX50, NY, USA) or confocal microscope (Zeiss LSM510 Meta, NY, USA or Nikon C1Si, NY, USA).

The immunoperoxidase procedure was done to analyze the levels of collagen IV (rabbit polyclonal, Abcam ab13966, 1:400), collagen VI (rabbit polyclonal, Santa Cruz sc-20649, 1:100), reticulin (rat monoclonal, Acris BM4018, 1:100), tenascin (rabbit polyclonal, Chemicon International AB19013, 1:500), cathepsin B (rabbit polyclonal, Upstate #06-480, 1:100), Lamp-1 (rat polyclonal, BD Pharmingen #553793, 1:100), Lamp-2 (rabbit polyclonal, Zymed #51-2200, 1:200) pax7 (mouse monoclonal, Developmental Studies Hybridoma Bank), and proliferating cell nuclear antigen (PCNA; rabbit polyclonal, Abcam ab15497, 1:200). Slides were washed in PBS and incubated for 30 min with blocking solution (1% BSA, 0.5% Tween-20, and 10% normal goat serum in PBS). Subsequently, the primary antibody was diluted in blocking solution, and slides were incubated overnight at 4 °C. The sections were then rinsed in PBS, incubated with biotinylated anti-mouse or anti-rabbit secondary antibodies for 60 min, rinsed in PBS, and reacted with ABC reagent (Vector Laboratories, Burlingame, CA) for 60 min. The endogenous peroxidase activity was quenched with 0.3% hydrogen peroxide in PBS for 30 min. The slides were rinsed in PBS and incubated with 3, 3′-diaminobenzidine substrate solution (DAB; Invitrogen) for 2 to 4 min. The reaction was stopped in distilled water and the slides were counterstained with H&E and examined on an Olympus microscope (Olympus BX50, NY, USA).

2.4. Western blot analysis

For western blot analysis, muscle fragments were homogenized with 5 volumes of RIPA buffer (10% SDS, 70 mmol/L Tris-HCl (pH 6.7), 10 mmol/L EDTA, and 5% β-mercaptoethanol) with phosphatase and protease inhibitor cocktails using a Dounce homogenizer. The homogenates were centrifuged at 13.000 ×*g* for 5 min at 4 °C, and the supernatants were transferred into new microtubes. The protein concentration was determined by optical density (OD = 595) using BSA solution; 25 μg *Neu1*$^{-/-}$ or *Neu1*$^{+/+}$ total protein underwent electrophoresis on SDS-PAGE gel (4%-12%). The gels were wet-blotted overnight at 4 °C against PVDF membranes. The membranes were blocked in TBS-Tween-20 containing 5% milk for 60 min and probed with primary antibody diluted in blocking solution overnight at 4 °C. The membranes were washed with TBS-Tween-20 and incubated with HRP–conjugated secondary antibodies for 1 h and developed by using SuperSignal West Femto Maximum Sensitivity Substrate (Thermo Scientific, Rockford, IL, USA). The antibodies used were as follow: anti-Lamp-1 (rat polyclonal, BD Pharmingen #553793, 1:500), anti-Lamp-2a and anti-Lamp-2b (gifts from Dr. Ana Maria Cuervo), anti–cathepsin B (rabbit polyclonal, Upstate #06-480, 1:2000), and anti-GAPDH (rabbit polyclonal, Chemicon International MAB374, 1:500).

2.5. Zymography

Gastrocnemius muscle from *Neu1*$^{-/-}$ and WT mice were homogenized in 5 volumes of PBS using a Dounce homogenizer and pelleted to remove non-solubilized components. Non-reducing sample buffer (62.5 mM Tris-HCl, pH 6.8, 25% glycerol, 4% SDS, 0.01% Bromophenol Blue) was added to increasing concentrations of both muscle lysates that were run on a 7.5% SDS-PAGE gel containing 1 mg/ml gelatin. The gel was incubated with renaturation buffer (2.5% Triton-X-100) for 30 min and development buffer (50 mM Tris-HCl, pH 7.5, 200 mM NaCl, 5 mM CaCl2, 0.02% Brij-35) overnight at 37 °C with one

change of buffer after 30 min. Bands were visualized as clear zones following staining with R250 Coomassie blue.

2.6. In situ zymography

In situ zymography was used to detect and localize net gelatinolytic and collagenolytic activity in *gastrocnemius* muscle sections of *Neu1*$^{-/-}$ and WT mice. Cryosections (10 μm) of muscle fragments were air-dried and overlaid with a solution containing 50 mM Tris–HCl, 5 mM CaCl, 0.2 mM sodium azide and 50 μg/ml fluorescence-labeled dye-quenched gelatin or dye-quenched collagen type I (Molecular Probes, Eugene, OR) and incubated overnight at 37 °C. Omission of the substrates served as a negative control. After three washes with PBS, slides were mounted in Vectashield mounting medium/DAPI (Vector, H1000).

For the analysis of collagen IV breakdown, the cryosections were overlaid with a buffer containing Collagen IV Oregon Green-488 (Molecular Probes), incubated for 2 h at 37 °C in a humidifying chamber, and fixed with 4% PFA. The slides were washed and mounted with Vectashield mounting medium/DAPI (Vector, H1000). As a control, the same experiment was performed using EDTA or omitting the substrate. The slides were examined under a fluorescent microscope (Olympus BX50) or confocal microscope (Zeiss LSM510 Meta).

2.7. Electron microscopy and semi-thin sectioning

For the electron microscopic studies, isolated *tibialis* and *gastrocnemius* muscles from *Neu1*$^{-/-}$ and WT mice were fixed in 4% glutaraldehyde, post-fixed in 1% OsO_4, and *en bloc* stained with 1% uranyl acetate. After standard dehydration, samples were infiltrated and embedded in Spurr low-viscosity resin (Electron Microscopy Sciences) and polymerized at 60 °C for 18 h. Semi-thin sections (0.5 μm) were stained with 1% toluidine blue. Sections (600–900 Å) were stained in grids with Reynolds lead citrate and uranyl acetate. The grids were analyzed in the Jeol “JEM-1200 EX-II” microscope with an AMT CCD camera.

2.8. Semi-quantitative RT-PCR

Total RNA was isolated from *gastrocnemius* muscles from *Neu1*$^{-/-}$ and WT mice (4–6 mo; n=3) using TRIZOL reagent (Invitrogen, Carlsbad, CA). The quantity of RNA was measured, and its purity was confirmed by spectroscopy. RNA was treated with amplification-grade DNAse I (Applied Biosystems/Ambion, Foster City, CA) to remove genomic DNA per the manufacturers’ instructions. First strand complementary DNA was produced using 1 μg of total RNA with a first strand cDNA Superscript II Reverse Transcriptase Kit (Invitrogen, Carlsbad, CA). cDNA was used as a template for the PCR in a 25-μl reaction volume including 2 μM of each primer, dNTPs (400 μM each), 2 mM $MgCl_2$, 2.5 ul Taq polymerase buffer (10x), and 0.625 Units Taq polymerase (Invitrogen), 29 cycles. Specific primers used are summarized in Suppl. table 1. Primer sequences for amplifications were designed based on published cDNA sequences. The PCR products were resolved on a 2% agarose gel containing 0.005% ethidium bromide and visualized with ultraviolet light. The intensity of the bands was calculated using ImageJ software (NIH) and normalized against *18S* or *β-actin* expression.

2.9. Cathepsin B deglycosylation assay

Fibroblasts were collected from *Neu1*$^{-/-}$ and WT muscle fragments, and equal numbers of cells were seeded in 35-mm plates and maintained in complete DMEM medium. At 100% confluence, the cells were harvested and lysed with RIPA buffer on ice for 30 min. The homogenates were centrifuged at 13,000 ×*g* for 5 min at 4 °C, and the supernatants were transferred into new microtubes. Enzymatic protein deglycosylation was performed using an

enzymatic deglycosylation kit (Prozyme, Hayward, CA) per the manufacturers' instructions. In brief, 60 μg lysate from *Neu1*$^{-/-}$ or *Neu1*$^{+/+}$ fibroblasts was incubated with N-glycanase, O-glycanase, sialidase I, or a combination of all three enzymes for 3 h at 37 °C. Samples were run on a Bis-Tris gradient gel (4%–12%), blotted against a PVDF membrane, and probed with a rabbit anti-cathepsin B antibody overnight at 4 °C.

2.10. Fibroblast exocytosis assay

An equivalent number of fibroblasts from *Neu1*$^{-/-}$ and WT mice were seeded in triplicate in 6-well plates. At 100% confluence, the medium (DMEM, pen-strep, GlutaMAX™, and 10% FBS) was replaced with 1 ml DMEM containing 1% BSA (w/v) with or without calcimycin (10 μM) and incubated for 2 h at 37 °C. The medium was collected and centrifuged to pellet the dead cells. The supernatant was stored at −80 °C. Enzyme activities were measured with the appropriate fluorometric or colorimetric substrates as previously described [7]. Cathepsins B and L were assayed using InnoZyme activity assay kits (EMD Biosciences, Madison, WI) per the manufacturers' instructions.

3. RESULTS

3.1. Increased number of fibroblast-like cells and expansion of ECM components in *Neu1*$^{-/-}$ skeletal muscle

Like children with the severe form of sialidosis (type II), *Neu1*$^{-/-}$ mice have growth delay and remain smaller than their WT littermates throughout their lifespan (approximately 6–8 mo) (Fig. 1A). Gross examination of the limb muscles revealed overt muscle atrophy (Fig. 1B) associated with progressive motor impairment. To determine the extent of the atrophic phenotype, we compared the weight of the *gastrocnemius* muscles isolated from *Neu1*$^{-/-}$ and WT mice of different ages. The muscle/body weight ratio (mg/g) of Neu1-deficient mice was significantly smaller than that of controls, and the disparity between the two phenotypes increased with age (Fig. 1C). Additionally**,** the cross-sectional area of the *Neu1*$^{-/-}$ *gastrocnemius* muscle was smaller than that of WT mice (Fig. 1D), confirming the occurrence of an atrophic phenotype.

Histologic examination of hematoxylin/eosin stained sections of skeletal muscle fascicles from 20 *Neu1*$^{-/-}$ mice (aged 2 weeks to 7 mo) identified extended areas of muscle connective tissue, preferentially in the epimysial and perimysial spaces, with increased cellularity and greatly augmented (ECM) compared to the WT sections (Figs. 2A and B). These severe abnormalities were detected throughout the length of the muscle, including the myotendinous junctions and tendons (Figs. 2D, F, and H) and were not observed in the WT littler mate control (Figs. 2C, E, G). Although intrusion of the ECM into the cytosol of the muscle fibers and thickening and digit-form appearance of the sarcolemma are normal characteristics of myotendinous junctions, in *Neu1*$^{-/-}$ mice these features were abnormally and ectopically present throughout the muscle and were accompanied by increased cellularity and extensive muscle fiber disruption (Figs. 2D and F). In young animals, the central areas of the fascicles were largely spared and maintained an overall normal appearance and organization; however, in mice older than 5 mo, the endomysial space was also expanded with increased cellularity. Different muscles i.e., *gastrocnemius*, *quadriceps*, *tibialis anterior*, *triceps brachialis*, and diaphragm showed similar histologic alterations, indicating a generalized skeletal muscle involvement in *Neu1*$^{-/-}$ mice.

To characterize better the hypercellularity observed in the abnormally expanded connective tissue, we first immunostained *Neu1*$^{-/-}$ muscle for immune cell markers (i.e., CD3, CD11b, and Ly-6G) (Fig. S1A). No positive reaction was detected in any muscle examined, indicating that immune cells did not contribute to the increased cellularity in the affected

areas. Similarly, staining with the satellite cells-specific marker Pax 7 did not identify an increased number of satellite cells in the affected muscle compared to the WT muscle (Fig. S1B). In contrast, a strong positive staining was obtained with an antibody against transcription factor 4, the earliest marker of developing muscle connective tissue [16], suggesting that these cells represent a population of fibroblast-like cells (Fig. 3A). Moreover, most of the fibroblast-like cells stained positive for proliferating cell nuclear antigen, a DNA-binding protein that is expressed during the S phase of the cell cycle (Fig. 3B), which indicates that the cells were actively dividing.

3.2. ECM components and proteolytic activity are increased in *Neu1*$^{-/-}$ skeletal muscle

Immunostaining of *Neu1*$^{-/-}$ muscle with antibodies against collagens III (reticulin), IV, and VI demonstrated prominent positivity in the infiltrated areas adjacent to the muscle fascicles (Fig. 4A). In addition, immunostaining for tenascin, which is highly expressed in the myotendinous junctions, showed aberrant distribution of this protein with large tenascin-positive areas extending into the endomysium (Fig. 4A, bottom right). By semi-quantitative RT-PCR, we also demonstrated increased levels of mRNA for collagens I, IV, and VI and laminin-α2 (Fig. 4B). These results demonstrated an overall increase in the synthesis of ECM components in the muscle-connective tissue of *Neu1*$^{-/-}$ mice.

Homeostasis of the ECM depends on the correct balance between synthesis and degradation of its components. Considering the observed accumulation of different types of collagens in the *Neu1*$^{-/-}$ ECM, we tested whether this phenotypic alteration was accompanied by deregulated activity of specific matrix metalloproteinases (MMPs) that are responsible for the remodeling and turnover of the ECM. Using gelatin zymography of total lysates of *quadriceps* muscle from *Neu1*$^{-/-}$ and WT mice, we detected a dramatic over-expression and activation of MMP2 and MMP9 (Fig. 5A). These two gelatinases normally degrade collagen IV and other collagens (V, VII and X) as well as basal lamina components, such as fibronectin and laminin. To assess the specific localization where the aberrantly increased MMP activity occurred, we performed gelatin and collagen IV *in situ* zymography on the *gastrocnemius*, *tibialis anterior* and *quadriceps* muscle tissues from *Neu1*$^{-/-}$ and WT mice. A substantial increase in the gelatinolytic and collagenolytic activity of MMPs was seen predominantly within the connective tissue infiltrates (Fig. 5B), and, most notably, within the muscle fibers adjacent to the expanded connective tissue (Fig. 5B, right panels).

We next tested whether the increased activity of MMPs was paralleled by an up-regulation of their corresponding mRNAs. Semi-quantitative RT-PCR showed a significant increase in MMP2 and MMP9 mRNA levels (Fig. 5C), together with massive accumulation of ECM components. Catalytic activation of MMPs in cells infiltrating the ECM occurs at the membrane and requires the activity of membrane-type MMPs and their inhibitors, tissue inhibitor of metalloproteinases 1 and 2 (TIMP1 and TIMP2). Indeed, we observed that the mRNAs for these proteins were also upregulated (Fig. 5C). Together, these results suggest that the profound alterations that occur in the perimysium and epimysium of *Neu1*$^{-/-}$ muscle as a consequence of Neu1 deficiency could have a deleterious effect on the juxtaposed myofibers.

3.3. *Neu1*$^{-/-}$ muscle fibers are infiltrated by fibroblast-like cells and ECM components at the epimysial and perimysial sites and undergo progressive degeneration

Analyses of toluidine blue–stained semi-thin sections of *Neu1*$^{-/-}$ muscle identified additional morphologic alterations present in the expanded epimysial and perimysial connective tissues and the adjacent muscle fibers (Fig. 6). Most of the proliferating fibroblast-like cells had a heavily vacuolated appearance due to the presence of numerous enlarged lysosomes in their cytoplasm (Fig. 6A), a feature that is diagnostic of a lysosomal

storage disease. At the site of the expanded connective tissue, the muscle fibers showed numerous invaginations of the sarcolemma and infiltration of the fibers by fibroblast-like cells and ECM components (Fig. 6B). In longitudinal sections, these invaginations or grooves extended the length of the myofibers (Figs. 6B and C) and were recognized in transverse sections as large vacuoles containing vacuolated cells and ECM material (Fig. 6D). As the disease progressed, infiltrated myofibers underwent complete cytosolic fragmentation, which was accompanied by gradual disruption of their cytoarchitecture (Figs. 6E and F).

These morphologic changes were particularly evident at the ultrastructural level (Fig. 7). Muscle fibers adjacent to the expanded perimysial area appeared grossly damaged by the infiltrating connective tissue (Figs. 7A-D). Fibroblast-like cells were filled with numerous storage-containing lysosomes (Figs. 7A-C). The sarcolemma of the muscle fibers extended into numerous digit-form invaginations containing ECM components (Fig. 7D, G and H). In addition, the sarcolemma appeared irregularly thickened (Fig. 7E). The progressive infiltration by the connective tissue caused extensive fragmentation of the myofibers (Figs. 7A and C). Individual fragments lost the normal muscle cytoarchitecture and displayed total disorganization of the sarcomeric apparatus and aggregation of Z lines (Fig. 7F).

In agreement with what observed at the ultrastructural level, immunofluorescent staining of *Neu1*$^{-/-}$ muscle sections with antibodies against the sarcolemmal proteins β-dystroglycan and dystrophin and the basal lamina protein laminin clearly highlighted the extent of fragmentation and destruction of the myofibers next to the perimysium (Fig. 8). In addition, the intensity of the fluorescent signal was greater in the affected areas than in the normal muscle fibers, suggesting intense remodeling of the sarcolemmal components probably in response to the increased proteolytic activity and ECM changes (Fig. 8). The fact that all three markers stained the membrane of the vacuole-like structures in these transverse sections confirmed that they resulted from invagination of the sarcolemma (Fig. 8).

We also analyzed the fiber composition of the *gastrocnemius*, *tibialis anterior*, and *quadriceps* muscles from WT and *Neu1*$^{-/-}$ mice using ATPase staining (data not shown) and immunofluorescence for different isoforms of myosin heavy chains i.e., MHC-2B, MHC-2A, and slow-MHC (data not shown). We did not detect any differences in fiber-type composition between WT and *Neu1*$^{-/-}$ mice, nor did we observe groups of atrophied fibers or angulated fibers. Thus, there was no evidence of denervation in the *Neu1*$^{-/-}$ muscle.

Interestingly, the skeletal muscle alterations observed in the *Neu1*$^{-/-}$ mice were also detected, albeit less prominently, in the *Ppca*-null mice, which have a secondary deficiency of Neu1 (Fig. S2), but were completely absent in *β-gal*-null mice (data not shown), which have normal Neu1 activity. From these experiments, we inferred that the skeletal muscle abnormalities in *Neu1*-null mice and *Ppca*-null mice are a direct consequence of the Neu1 deficiency.

3.4. Regeneration and apoptosis/necrosis do not occur in the *Neu1*$^{-/-}$ skeletal muscle

Considering the extensive muscle destruction in *Neu1*$^{-/-}$ mice, we predicted that regenerative and necrotic processes would occur in the affected muscle. This assumption was also justified by the presence of central nuclei in a few fibers adjacent to the most damaged areas (Fig. S3A). Interestingly, however, there were no signs of overt necrosis in the *Neu1*$^{-/-}$ muscle at the histopathologic level (Fig. 2). In addition, immunofluorescent staining of muscle sections with an antibody against embryonic myosin heavy chain did not detect *de novo* formation of myofibers (data not shown). Finally, as mentioned above, immunostaining for Pax7 and MyoD, both markers of satellite cell activation, did not

identify any positive cells (Fig. S1B and data not shown), reiterating the absence of active regeneration in the *Neu1*$^{-/-}$ muscle.

We then determined whether *Neu1*$^{-/-}$ myofibers or fibroblast-like cells underwent cell death using a TUNEL assay, which labels DNA fragments generated during apoptosis, necrosis [17], or lysosomal digestion [18]. Less than 1% of the cells in the expanded connective tissue and the infiltrated muscle fibers were TUNEL-positive (Fig. S3B) even in regions outside the myotendinous junctions. These data support the notion that the *Neu1*$^{-/-}$ muscle fibers undergo a different mechanism of degeneration not related to apoptosis.

3.5. *Neu1*$^{-/-}$ myofibers maintain sarcolemmal integrity

Low molecular weight dyes such as Evans blue strongly stain the interstitial spaces within the connective tissue and between skeletal muscle fibers. Therefore, the presence of such dyes inside myofibers is considered a reliable indicator of sarcolemmal damage or fiber degeneration [19]. After injection of Evans blue dye in *Neu1*$^{-/-}$ mice, only the muscle fibers immediately adjacent to the expanded connective tissue showed intense fluorescent signal in their cytosol. This staining was similar to the signal detected in the connective tissue ECM, which indicated that it was the result of invagination of the fibers by ECM components rather than increased sarcolemmal permeability (Fig. S4). Increased serum levels of muscle proteins, such as creatine kinase, which are normally restricted to the myofiber cytosol, usually accompany the disruption of myofiber integrity. However, the level of serum creatine kinase measured in *Neu1*$^{-/-}$ mice was normal (not shown), further indicating that the sarcolemma was not damaged in *Neu1*$^{-/-}$ myofibers.

3.6. Altered pattern of expression of lysosomal markers in the ECM of *Neu1*$^{-/-}$ skeletal muscle

We have previously shown that Neu1 activity is pivotal for the processing of sialic acids on the structural lysosomal proteins Lamp-1 and Lamp-2 and proteolytic enzymes such as the cathepsins [7]. We have also demonstrated that Neu1 is a negative regulator of lysosomal exocytosis in the *Neu1*$^{-/-}$ bone marrow and cochlear marginal cells [7,20]. We therefore investigated the contribution of these lysosomal proteins and the process of lysosomal exocytosis to the severe muscle and connective tissue phenotype of *Neu1*$^{-/-}$ mice. Immunohistochemical analysis of the *gastrocnemius* muscle from *Neu1*$^{-/-}$ mice showed strong positivity for Lamp proteins and cathepsin B in the areas of connective tissue infiltration and the juxtaposed myofibers, which was absent in the WT control (Fig. 9A middle and left panels). Increased levels of these proteins were also seen in the endomysial space and most importantly within the myofibers (Fig. 9A, right panels).

These results were confirmed by immunoblot analyses, which demonstrated increased amounts of Lamp-1, Lamp-2a and b, and cathepsin B in total muscle lysates from *Neu1*$^{-/-}$ mice (Fig. 9B). In addition, these proteins had a distinct migration pattern compared to that in WT tissues, confirming both Lamp-1 and Lamp-2 are over-sialylated in the absence of Neu1 activity [7]. The altered migration pattern and increased amount of cathepsin B in *Neu1*$^{-/-}$ muscle suggested that this protein was also over-sialylated. This was confirmed by *in vitro* enzymatic removal of all N-glycans on cathepsin B, which released a core protein identical in molecular weight in *Neu1*$^{-/-}$ and WT fibroblast lysates, indicating that cathepsin B is a natural substrate of Neu1 (Fig. 9C).

3.7. *Neu1*$^{-/-}$ fibroblasts show increased exocytosis

We demonstrated previously that in skin fibroblasts from patients with type II sialidosis the levels of Lamp-1 is increased at the PM and this is accompanied by higher extracellular activity of α-mannosidase [7]. These findings suggest that even in non-secretory cells loss of

Neu1 activity results in increased lysosomal exocytosis. In support of this notion, we now measured higher α-mannosidase, cathepsins B and L activities in the culture medium of fibroblasts isolated from *Neu1*$^{-/-}$ muscle (Fig. 9D), indicating that these cells undergo excessive lysosomal exocytosis, closely reproducing the phenotypic alterations found in human patient fibroblasts.

4. DISCUSSION

Here we describe an unusual muscle phenotype in mice deficient for the lysosomal enzyme Neu1. The abnormalities are characterized by dramatic expansion of the epimysial and perimysial connective tissues with increased cellularity and ECM components. These features are accompanied by progressive infiltration of proliferating fibroblast-like cells and connective tissue ECM into the adjacent muscle fibers, which ultimately lead to extreme cytosolic fragmentation and myofiber degeneration. This atypical muscle phenotype defines a new pathogenic model for muscle diseases, and explains, in part, the neuromuscular manifestations seen in patients with type II sialidosis, such as hypotonia, muscle atrophy, weakness, and osteoskeletal deformities [5]. In future, analysis of muscle biopsies from sialidosis patients with different clinical phenotypes would allow us to verify this hypothesis.

A primary deficiency of lysosomal proteins has been associated with different forms of skeletal muscle abnormalities [21]. However, the phenotypic features identified in Neu1-deficient mice appear to differ from those present in other lysosomal muscle diseases, which are mostly associated with aberrant autophagic activity. For instance, deficiency of the enzyme α-glucosidase in Pompe disease results in severe cardiac failure and muscle wasting [22]. The hallmark of this disorder is the presence of large glycogen-filled lysosomes in tissues, but it is the accumulation of autophagic debris and autophagosome formation that mostly contribute to muscle weakness [23]. Similarly, Danon disease, caused by LAMP-2 deficiency, is characterized by hypertrophic cardiomyopathy, myopathy, and mental retardation [21]. Muscle biopsies from these patients have revealed increased number of scattered intracytoplasmic vacuoles with sarcolemmal features and autophagic appearance [21,24]. Other rare forms of autophagic myopathies have been described, but their primary defects remain unknown [21].

Similarly to our Neu1-deficient mice, *synaptotagmin VII (SytVII)*–null mice present with extensive fibrosis in the skin and skeletal muscle. SytVII is the Ca2+ sensor component of the multiprotein complex that promotes the fusion of the lysosomal membrane with the PM, which is followed by the release of the lysosomal content into the ECM [25]. In contrast to our mice that have increased lysosomal exocytosis, *SytVII*-null mice have impaired lysosomal exocytosis and PM repair, which promotes the leakage of cytosolic content into the extracellular space. Consequently, these mice develop an inflammatory myopathy with an antinuclear antibody response characteristic of autoimmune disorders [26], features not detected in the Neu1-deficient mice.

The absence of an inflammatory response in the *Neu1*$^{-/-}$ muscle suggests that muscle degeneration in these mice is not due to the release of cytosolic constituents into the ECM. Only those muscle fibers juxtaposed to the expanded connective tissue showed increased Evans blue dye signal, which is apparently caused by connective tissue infiltration rather than sarcolemmal damage. Moreover, serum creatine kinase levels, another marker of muscle fiber damage, were normal in all animals tested. However, it is unknown whether creatine kinase levels are normal or elevated in patients with sialidosis. Finally, we did not observe a significant number of newly formed myofibers with centrally located nuclei or fibers expressing embryonic forms of myosin heavy chain, which would indicate activation

of the satellite cells, an event that normally occurs after muscle lesion. Together, these observations strongly support the notion that myofiber sarcolemmal damage is not a significant event associated with the degeneration of *Neu1*$^{-/-}$ skeletal muscle. This justifies the absence of muscle necrosis, which is the hallmark of muscular dystrophies.

To explain the muscle phenotype in *Neu1*$^{-/-}$ mice, we reason that the loss of Neu1 activity changes the ECM environment. Impaired processing of sialic acid on the glycans of as yet unknown targets of Neu1 may affect the biochemical properties of the ECM. In line with this assumption is a recent report by [27], which suggests that Neu1 plays an important role in the downregulation of arterial smooth muscle cell proliferation. Using neuraminidase inhibitors, these authors showed that Neu1 activity at the PM could structurally alter the sialic acid content of cell surface receptors, thereby decreasing the net cellular responsiveness to their respective mitogenic ligands. Although the mechanisms that mediate the proliferation of fibroblast-like cells in *Neu1*$^{-/-}$ muscle remain to be elucidated, the data presented here suggest the involvement of lysosomal enzymes, in particular Neu1, in the control of cell proliferation and ECM remodeling.

It is tempting to speculate that the enhanced proliferation and infiltration of the fibroblast-like cells in *Neu1*$^{-/-}$ mice share mechanistic features with the same processes observed in cancer cells. Indeed, there is evidence that cancer cells undergo alterations in glycosylation and sialylation of cell surface molecules, which appear to contribute to malignant transformation, thereby increasing their metastatic potential and invasiveness [28]. These phenotypic alterations are mirrored by changes in the expression pattern of endogenous sialidases [29]. In particular, there seems to be an inverse correlation between levels of NEU1 activity and the potential of tumor cells to proliferate, migrate and invade in *in vitro* assays and xerographs [29–31]. In addition, *NEU1* overexpression also results in downregulation of MMPs, which are induced in cancer cells with high metastatic potential. These proteases comprise a family of zinc-dependent enzymes that, together with their inhibitors, the TIMPs, are the major physiological regulators of the turnover of the ECM [32]. MMPs have been implicated in the dissemination of cancer cells by breaking down the ECM, but they are also important in creating an environment that supports the initiation and maintenance of growth of primary and metastatic tumors [33,34]. Interestingly, we observed also in *Neu1*$^{-/-}$ connective tissue-infiltrated muscle fibers a strong upregulation of MMPs (MMP-2 and MMP-9), both at the protein and mRNA levels. The strong correlation between the low-expression levels of NEU1, the remodeling of the ECM by MMPs, and the high rate of proliferation and invasion of colon carcinoma cells, seems to be recapitulated in the muscle-connective tissue of *Neu1*$^{-/-}$ mice. The activation of MMPs in the muscle of these mice might facilitate the migration of fibroblast-like cells and their infiltration into muscle fibers, quite similarly to what observed during metastatic cancer progression.

Besides their involvement in cancer, excess production of MMPs leads to pathology in a wide range of other tissues [35]. Increased expression of MMPs has been reported in atrophic skeletal muscle, muscular dystrophies, and in inflammatory myopathies [36–38]. Many studies have demonstrated that a key process in the infiltration of mononuclear cells and tissue destruction in inflammatory disorders of the muscle may be associated with the MMP-mediated proteolytic disruption of the ECM components, such as basement lamina and sarcolemma [36,38]. In this respect it is remarkable that we observed no increase in inflammatory markers or cells in the connective tissue-infiltrated muscles of *Neu1*$^{-/-}$ mice. Nevertheless, we have no indication that inflammation is suppressed in the muscle of *Neu1*$^{-/-}$ mice because cardiotoxin treated, denervated muscle tissue showed no impairment in the inflammatory response (data not shown).

It is noteworthy that even with the marked increase of proteolytic activity in the ECM, components of the basement membrane (laminin, collagen IV) and the sarcolemma (dystrophin and β-dystroglycans) appear to accumulate in muscle fibers juxtaposed to the affected areas. We speculate that the accumulation of these proteins may be part of an adaptive mechanism to preserve the integrity of the sarcolemma, thereby avoiding muscle necrosis and extrusion of cytosolic components into the extracellular space. Thus, the activation of MMPs in the ECM of *Neu1*$^{-/-}$ mice may have two opposing consequences: (i) It appears to structurally and physiologically alter the basement membrane and sarcolemma of myofibers to facilitate the invagination by cells and connective tissue localized in the ECM, and (ii) it may induce an adaptive mechanism to preserve the attachment between the sarcolemma and the ECM. However, ultimately this adaptive mechanism is not sufficient to avoid the progressive muscle fiber fragmentation and degeneration observed in these mice.

In conclusion, the unique pattern of muscle fiber disruption/degeneration and connective tissue expansion and proliferation observed in this animal model of sialidosis implicates Neu1 deficiency in the deregulation of cell proliferation and ECM remodeling. These findings will help us to gain insight into the neuromuscular manifestations reported in patients with sialidosis.

Supplementary Material

Refer to Web version on PubMed Central for supplementary material.

Acknowledgments

We wish to thank Mehmet Kocak for critical help in the statistical analyses, Simon Moshiach for confocal imaging, and Leandro Lo Cascio for his technical assistance in the MMPs experiments. We are indebted to Gabrielle Kardon for advise on the TCF-4 staining. A.d'A. holds an endowed chair in Genetics from the Jewelry Charity Fund. This work was supported in part by the NIH grants GM60950 and DK52025, the Assisi Foundation of Memphis and the American Syrian Associated Charities (ALSAC) of SJCRH.

Abbreviations

Neu1	neuraminidase 1
PPCA	protective protein/cathepsin A
Lamp-1	lysosomal-associated membrane protein-1
MMP	matrix metalloproteinase
TIMP	tissue inhibitors of metalloproteinases
PM	plasma membrane
SytVII	synaptotagmin VII

References

1. Bonten E, van der Spoel A, Fornerod M, Grosveld G, d'Azzo A. Characterization of human lysosomal neuraminidase defines the molecular basis of the metabolic storage disorder sialidosis. Genes Dev 1996;10:3156–3169. [PubMed: 8985184]
2. van der Spoel A, Bonten E, d'Azzo A. Transport of human lysosomal neuraminidase to mature lysosomes requires protective protein/cathepsin A. EMBO J 1998;17:1588–1597. [PubMed: 9501080]
3. Thomas, GH. Disorders of glycoprotein degradation and structure: a-mannosidosis, b-mannosidosis, fucosidosis, and sialidosis. In: Scriver, CR.; Beaudet, AL.; Sly, WS.; Valle, D., editors. The

Metabolic and Molecular Bases of Inherited Disease. Vol. III. McGraw Hill, Inc; New York: 2001. p. 3507-3534.

4. d'Azzo, A.; Andria, G.; Strisciuglio, P.; Galjaard, H. Galactosialidosis. In: Scriver, C.; Beaudet, A.; Sly, W.; Valle, D., editors. The Metabolic and Molecular Bases of Inherited Disease. Vol. 3. McGraw-Hill Publishing Co; New York: 2001. p. 3811-3826.
5. Bonten EJ, Arts WF, Beck M, Covanis A, Donati MA, Parini R, Zammarchi E, d'Azzo A. Novel mutations in lysosomal neuraminidase identify functional domains and determine clinical severity in sialidosis. Hum Mol Genet 2000;9:2715–2725. [PubMed: 11063730]
6. de Geest N, Bonten E, Mann L, de Sousa-Hitzler J, Hahn C, d'Azzo A. Systemic and neurologic abnormalities distinguish the lysosomal disorders sialidosis and galactosialidosis in mice. Hum Mol Genet 2002;11:1455–1464. [PubMed: 12023988]
7. Yogalingam G, Bonten EJ, van de Vlekkert D, Hu H, Moshiach S, Connell SA, d'Azzo A. Neuraminidase 1 is a negative regulator of lysosomal exocytosis. Dev Cell 2008;15:74–86. [PubMed: 18606142]
8. Andrews NW. Regulated secretion of conventional lysosomes. Trends Cell Biol 2000;10:316–321. [PubMed: 10884683]
9. Caciotti A, Donati MA, Bardelli T, d'Azzo A, Massai G, Luciani L, Zammarchi E, Morrone A. Primary and secondary elastin-binding protein defect leads to impaired elastogenesis in fibroblasts from GM1-gangliosidosis patients. Am J Pathol 2005;167:1689–1698. [PubMed: 16314480]
10. Malvagia S, Morrone A, Caciotti A, Bardelli T, d'Azzo A, Ancora G, Zammarchi E, Donati MA. New mutations in the PPBG gene lead to loss of PPCA protein which affects the level of the beta-galactosidase/neuraminidase complex and the EBP-receptor. Mol Genet Metab 2004;82:48–55. [PubMed: 15110321]
11. Hinek A, Pshezhetsky AV, von Itzstein M, Starcher B. Lysosomal sialidase (neuraminidase-1) is targeted to the cell surface in a multiprotein complex that facilitates elastic fiber assembly. J Biol Chem 2006;281:3698–3710. [PubMed: 16314420]
12. Starcher B, d'Azzo A, Keller PW, Rao GK, Nadarajah D, Hinek A. Neuraminidase-1 is required for the normal assembly of elastic fibers. Am J Physiol Lung Cell Mol Physiol 2008;295:L637–647. [PubMed: 18689602]
13. Canty EG, Kadler KE. Procollagen trafficking, processing and fibrillogenesis. J Cell Sci 2005;118:1341–1353. [PubMed: 15788652]
14. Sanes JR. The basement membrane/basal lamina of skeletal muscle. J Biol Chem 2003;278:12601–12604. [PubMed: 12556454]
15. Winder SJ. The complexities of dystroglycan. Trends Biochem Sci 2001;26:118–124. [PubMed: 11166570]
16. Kardon G, Harfe BD, Tabin CJ. A Tcf4-positive mesodermal population provides a prepattern for vertebrate limb muscle patterning. Dev Cell 2003;5:937–944. [PubMed: 14667415]
17. Grasl-Kraupp B, Ruttkay-Nedecky B, Koudelka H, Bukowska K, Bursch W, Schulte-Hermann R. In situ detection of fragmented DNA (TUNEL assay) fails to discriminate among apoptosis, necrosis, and autolytic cell death: a cautionary note. Hepatology 1995;21:1465–1468. [PubMed: 7737654]
18. McIlroy D, Tanaka M, Sakahira H, Fukuyama H, Suzuki M, Yamamura K, Ohsawa Y, Uchiyama Y, Nagata S. An auxiliary mode of apoptotic DNA fragmentation provided by phagocytes. Genes Dev 2000;14:549–558. [PubMed: 10716943]
19. Hamer PW, McGeachie JM, Davies MJ, Grounds MD. Evans Blue Dye as an in vivo marker of myofibre damage: optimising parameters for detecting initial myofibre membrane permeability. J Anat 2002;200:69–79. [PubMed: 11837252]
20. Wu X, Steigelman KA, Bonten E, Hu H, He W, Ren T, Zuo J, d'Azzo A. Vacuolization and alterations of lysosomal membrane proteins in cochlear marginal cells contribute to hearing loss in neuraminidase 1-deficient mice. Biochim Biophys Acta 2010;1802:259–268. [PubMed: 19857571]
21. Nishino I. Autophagic vacuolar myopathy. Semin Pediatr Neurol 2006;13:90–95. [PubMed: 17027858]

22. Bembi B, Cerini E, Danesino C, Donati MA, Gasperini S, Morandi L, Musumeci O, Parenti G, Ravaglia S, Seidita F, Toscano A, Vianello A. Diagnosis of glycogenosis type II. Neurology 2008;71:S4–11. [PubMed: 19047572]
23. Raben N, Roberts A, Plotz PH. Role of autophagy in the pathogenesis of Pompe disease. Acta Myol 2007;26:45–48. [PubMed: 17915569]
24. Sugie K, Noguchi S, Kozuka Y, Arikawa-Hirasawa E, Tanaka M, Yan C, Saftig P, von Figura K, Hirano M, Ueno S, Nonaka I, Nishino I. Autophagic vacuoles with sarcolemmal features delineate Danon disease and related myopathies. J Neuropathol Exp Neurol 2005;64:513–522. [PubMed: 15977643]
25. Andrews NW, Chakrabarti S. There's more to life than neurotransmission: the regulation of exocytosis by synaptotagmin VII. Trends Cell Biol 2005;15:626–631. [PubMed: 16168654]
26. Chakrabarti S, Kobayashi KS, Flavell RA, Marks CB, Miyake K, Liston DR, Fowler KT, Gorelick FS, Andrews NW. Impaired membrane resealing and autoimmune myositis in synaptotagmin VII-deficient mice. J Cell Biol 2003;162:543–549. [PubMed: 12925704]
27. Hinek A, Bodnaruk TD, Bunda S, Wang Y, Liu K. Neuraminidase-1, a subunit of the cell surface elastin receptor, desialylates and functionally inactivates adjacent receptors interacting with the mitogenic growth factors PDGF-BB and IGF-2. Am J Pathol 2008;173:1042–1056. [PubMed: 18772331]
28. Dennis JW, Granovsky M, Warren CE. Glycoprotein glycosylation and cancer progression. Biochim Biophys Acta 1999;1473:21–34. [PubMed: 10580127]
29. Miyagi T, Wada T, Iwamatsu A, Hata K, Yoshikawa Y, Tokuyama S, Sawada M. Molecular cloning and characterization of a plasma membrane-associated sialidase specific for gangliosides. J Biol Chem 1999;274:5004–5011. [PubMed: 9988745]
30. Miyagi T, Wada T, Yamaguchi K, Shiozaki K, Sato I, Kakugawa Y, Yamanami H, Fujiya T. Human sialidase as a cancer marker. Proteomics 2008;8:3303–3311. [PubMed: 18651674]
31. Uemura T, Shiozaki K, Yamaguchi K, Miyazaki S, Satomi S, Kato K, Sakuraba H, Miyagi T. Contribution of sialidase NEU1 to suppression of metastasis of human colon cancer cells through desialylation of integrin beta4. Oncogene 2009;28:1218–1229. [PubMed: 19151752]
32. McCawley LJ, Matrisian LM. Matrix metalloproteinases: they're not just for matrix anymore. Curr Opin Cell Biol 2001;13:534–540. [PubMed: 11544020]
33. Chambers AF, Matrisian LM. Changing views of the role of matrix metalloproteinases in metastasis. J Natl Cancer Inst 1997;89:1260–1270. [PubMed: 9293916]
34. Nakada M, Nakamura H, Ikeda E, Fujimoto N, Yamashita J, Sato H, Seiki M, Okada Y. Expression and tissue localization of membrane-type 1, 2, and 3 matrix metalloproteinases in human astrocytic tumors. Am J Pathol 1999;154:417–428. [PubMed: 10027400]
35. Birkedal-Hansen H, Moore WG, Bodden MK, Windsor LJ, Birkedal-Hansen B, DeCarlo A, Engler JA. Matrix metalloproteinases: a review. Crit Rev Oral Biol Med 1993;4:197–250. [PubMed: 8435466]
36. Choi YC, Dalakas MC. Expression of matrix metalloproteinases in the muscle of patients with inflammatory myopathies. Neurology 2000;54:65–71. [PubMed: 10636127]
37. Kherif S, Lafuma C, Dehaupas M, Lachkar S, Fournier JG, Verdière-Sahuqué M, Fardeau M, Alameddine HS. Expression of matrix metalloproteinases 2 and 9 in regenerating skeletal muscle: a study in experimentally injured and mdx muscles. Dev Biol 1999;205:158–170. [PubMed: 9882504]
38. Kieseier BC, Schneider C, Clements JM, Gearing AJ, Gold R, Toyka KV, Hartung HP. Expression of specific matrix metalloproteinases in inflammatory myopathies. Brain 2001;124:341–351. [PubMed: 11157561]
39. Harumiya S, Gibson MA, Koshihara Y. Antisense suppression of collagen VI synthesis results in reduced expression of collagen I in normal human osteoblast-like cells. Biosci Biotechnol Biochem 2002;66:2743–2747. [PubMed: 12596881]
40. Juárez P, Vilchis-Landeros MM, Ponce-Coria J, Mendoza V, Hernández-Pando R, Bobadilla NA, López-Casillas F. Soluble betaglycan reduces renal damage progression in db/db mice. Am J Physiol Renal Physiol 2007;292:321–329.

41. Inoue S, Nakazawa T, Cho A, Dastvan F, Shilling D, Daum G, Reidy M. Regulation of arterial lesions in mice depends on differential smooth muscle cell migration: a role for sphingosine-1-phosphate receptors. J CVasc Surg 2008;46:756–763.

42. Takenaka H, Kihara Y, Iwanaga Y, Onozawa Y, Toyokuni S, Kita T. Angiotensin II, oxidative stress, and extracellular matrix degradation during transition to LV failure in rats with hypertension. J Mol Cell Cardiol 2006;41:989–997. [PubMed: 16979182]

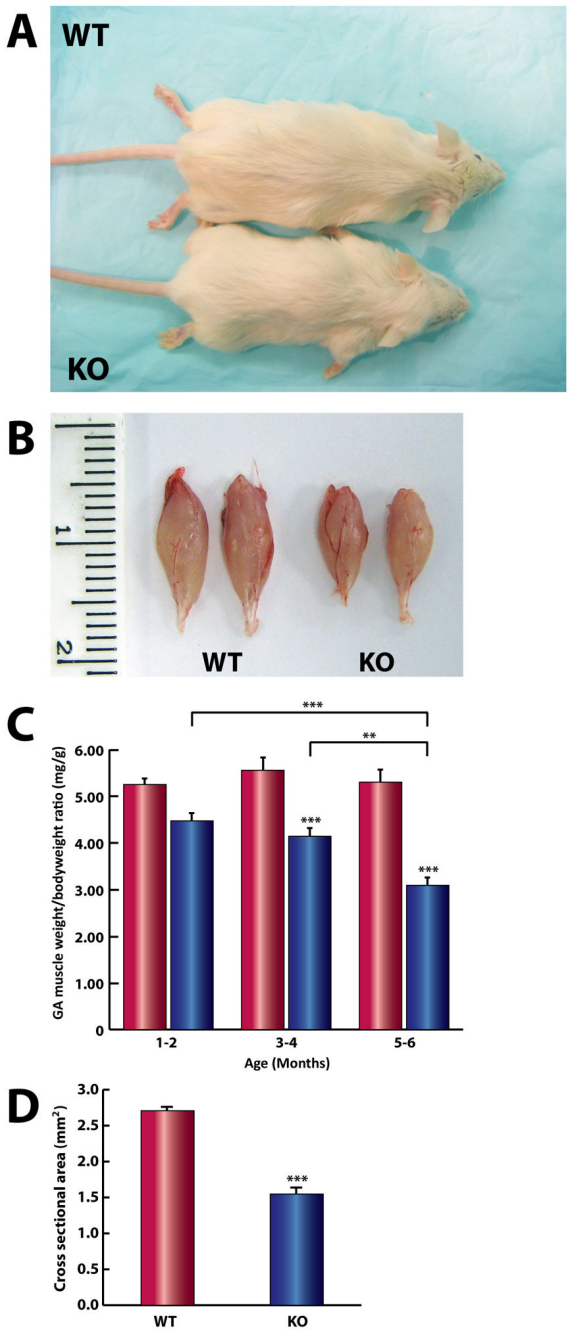

Fig. 1.

Growth retardation and progressive skeletal muscle atrophy in *Neu1*$^{-/-}$ mice. **(A)** A comparison of a representative 4 mo old male *Neu1*$^{-/-}$ mouse (KO) and its WT littermate. **(B)** Atrophic *gastrocnemius* muscles of KO and WT mice. **(C)** The ratios of *gastrocnemius* muscle weight per body weight at different ages shows significant, progressive wasting of KO muscles (blue; 1–2 mo [n=6], 3–4 mo [n=5], and 5–6 mo [n=5]) compared to WT tissues (red; 1–2 mo [n=8], 3–4 mo [n=4], and 5–6 mo [n=5]) (** = $p<0.01$, *** = $p<0.001$; Two-way ANOVA). **(D)** The average fiber cross-sectional area of KO gastrocnemius muscle (1.54 mm^2, n=3; 3 fields each) was significantly less than that of their age-matched controls (2.70 mm^2, n=3; 3 fields each) (*** = $p<0,001$; Student's t-test).

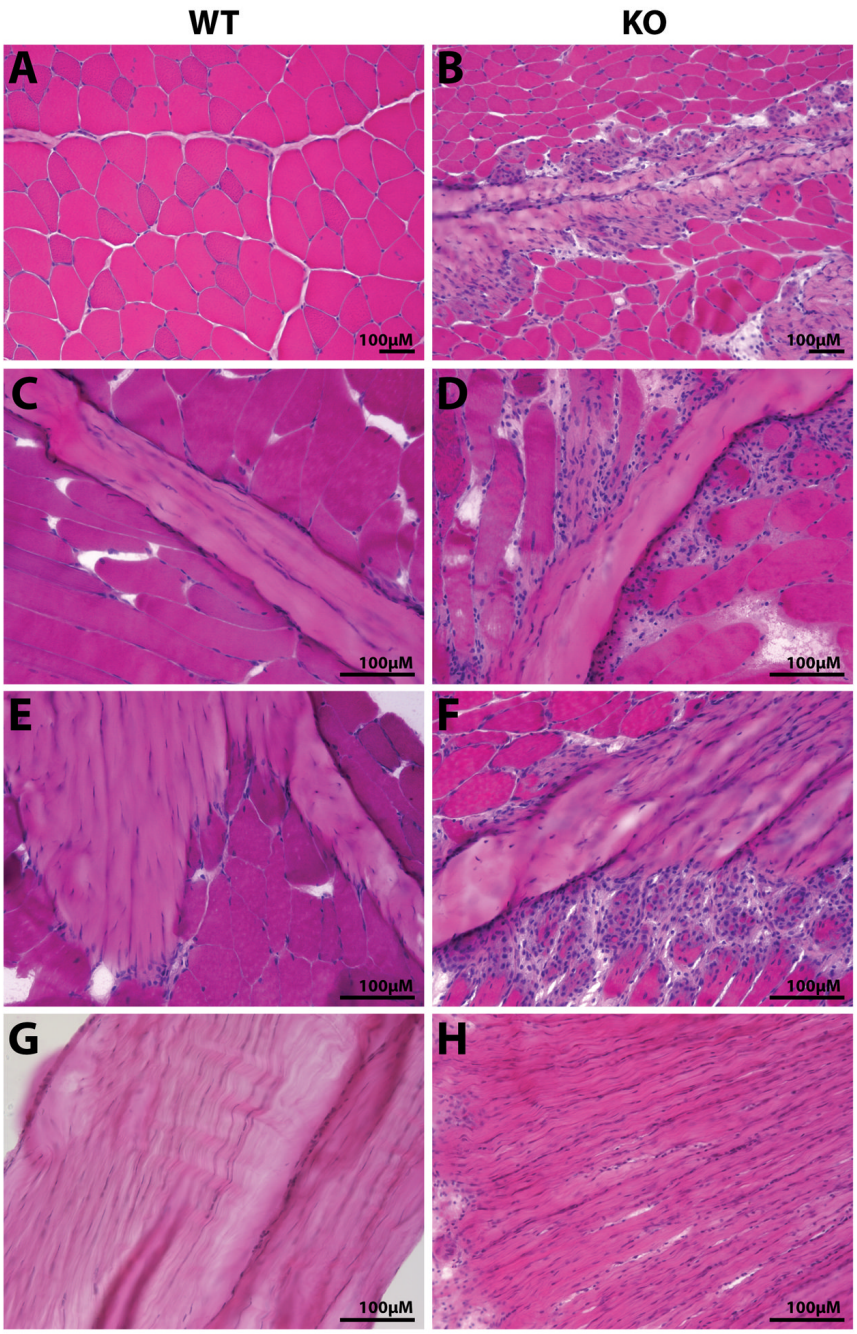

Fig. 2.

H&E staining of transverse sections of *Neu1*$^{-/-}$ (KO) *gastrocnemius* muscle. This analysis shows the presence of large areas of connective tissue infiltrates and increased number of cells in **(B)** the epimysium and perimysium spaces, **(D and F)** myotendinous junction and **(H)** tendon. Normal histology of **(A)** *gastrocnemius* muscle, **(C and E)** myotendinous junction, and **(G)** tendon from a WT mouse.

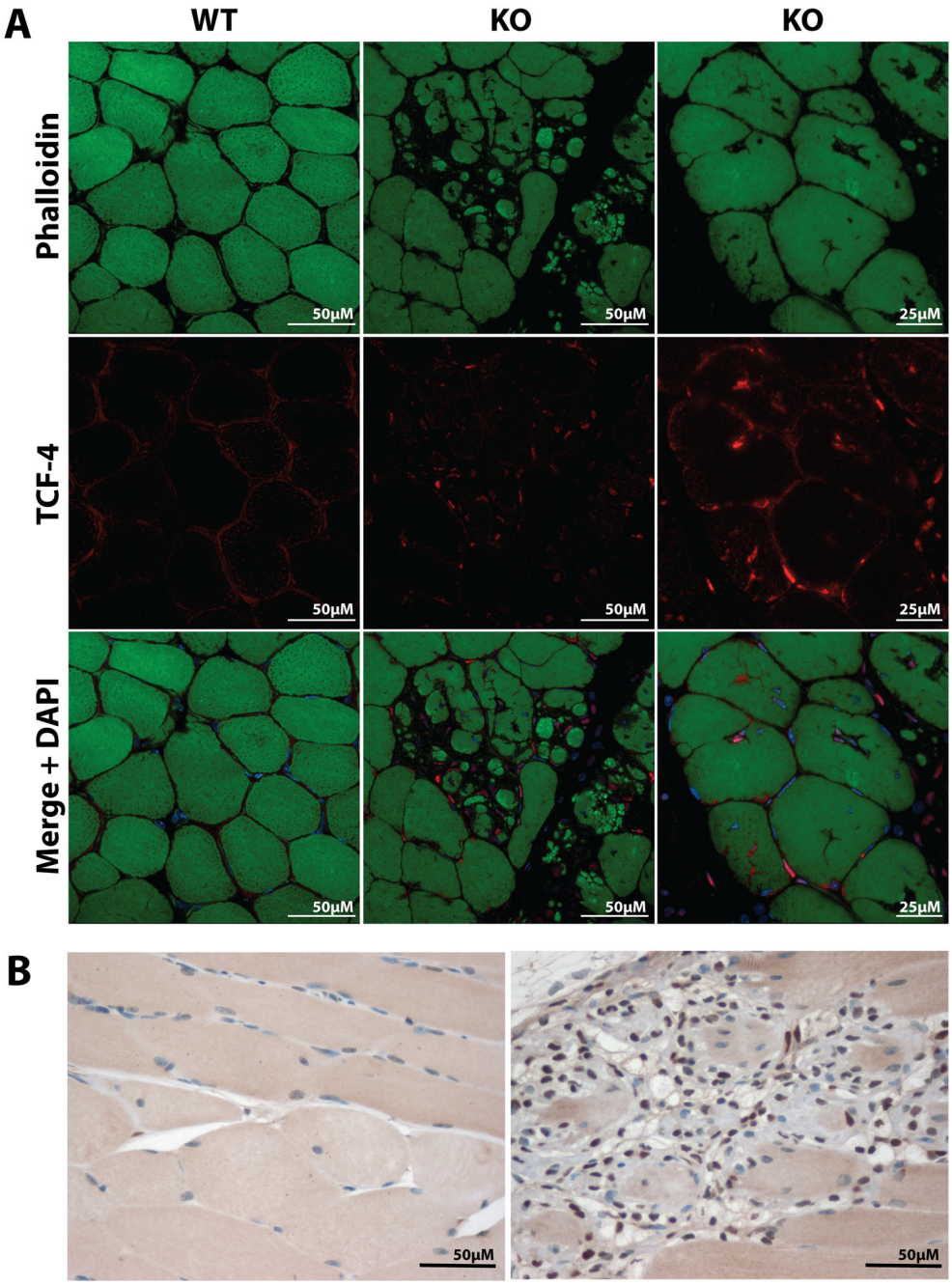

Fig. 3.

Confocal analysis of sections from *Neu1*$^{-/-}$ (KO) and WT *gastrocnemius* muscle. **(A)** Images show that most cells located at the infiltrated connective tissue and within the adjacent muscle fibers are transcription factor-4-positive (phalloidin, top panels shown in green; transcription factor-4, middle panels shown in red; bottom panels merge and DAPI shown in blue). **(B)** Immunoperoxidase staining of similar segments revealed that the cells are also proliferating cell nuclear antigen-positive (brown).

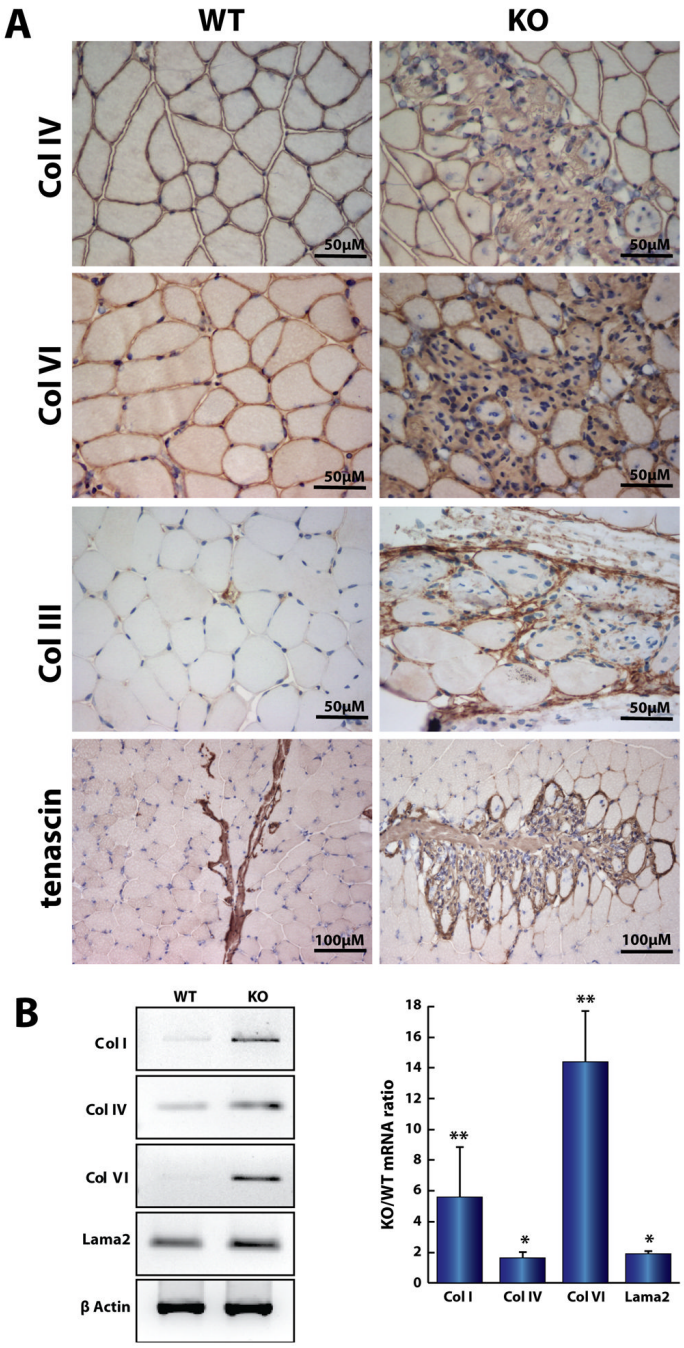

Fig. 4.

ECM components accumulate in *Neu1*$^{-/-}$ (KO) *gastrocnemius* muscle. **(A)** Immunohistochemical analysis showed that collagen IV, VI, Collagen III (reticulin), and tenascin prominently mark the KO perimysial region. **(B)** Semi quantitative RT-PCR of total RNA from KO and WT *gastrocnemius* muscles demonstrated a significant increase in the expression of collagens I (n=3), IV (n=6), VI (n=3) and laminin-α2 (Lama2; n=3)) in the KO muscle (* = $p<0.05$; ** = $p<0.01$; Student's t test), indicating an overall increase on the synthesis of the ECM proteins.

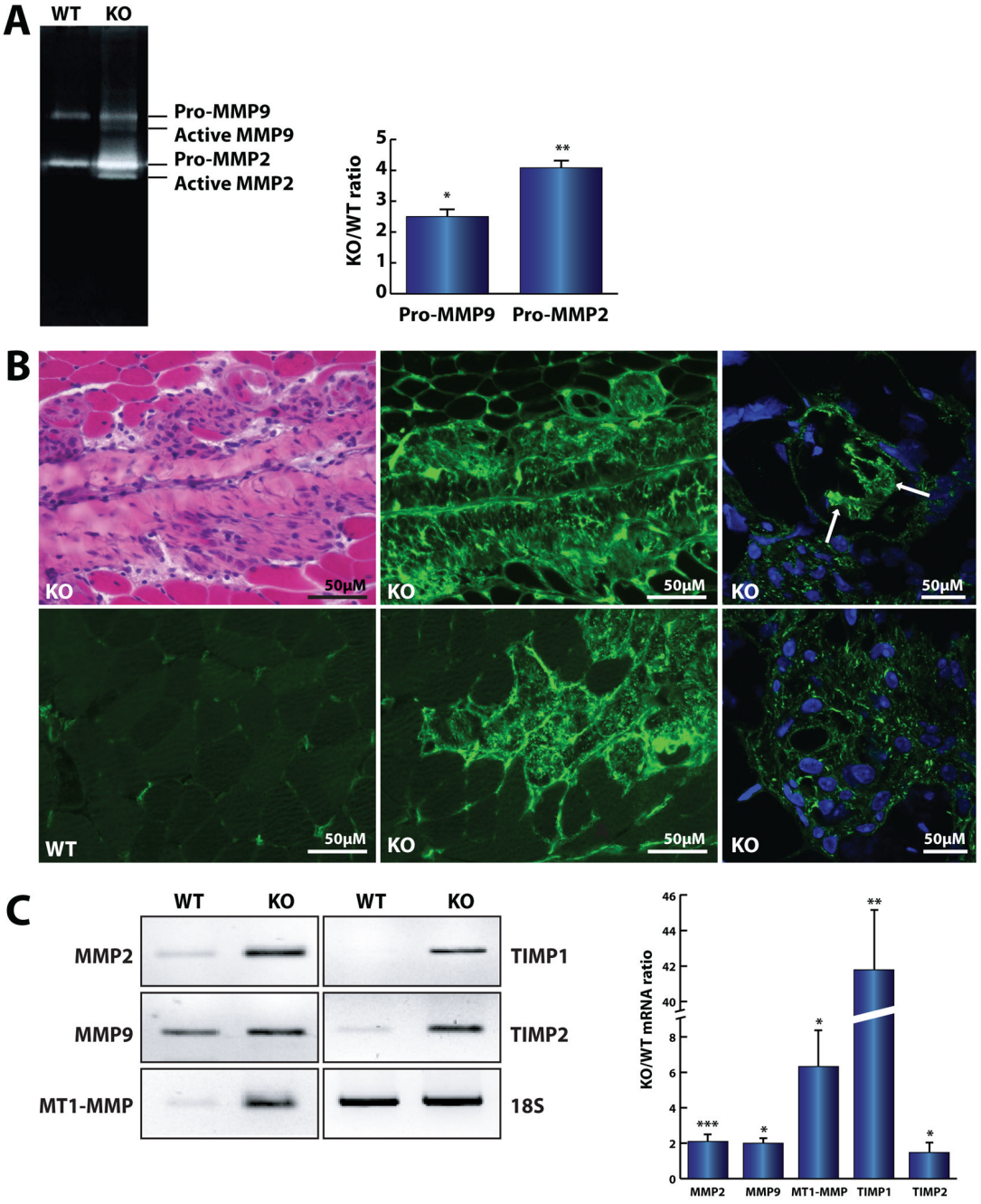

Fig. 5.

Increased activity mediated by MMPs in the ECM of *Neu1*$^{-/-}$ (KO) skeletal muscle. **(A)** Zymography of the total lysate from KO (n=3) and WT (n=3) *quadriceps* muscles showed a higher activity of MMP2 and MMP9 in the KO mice. **(B)** The gelatin (top middle) and collagen IV (bottom left and middle) *in situ* zymography revealed an increase in gelatinolytic and collagenolytic activity in the affected areas of KO *gastrocnemius* muscle, respectively. Confocal images showed increased gelatinolytic activity within the infiltrated muscle fibers (arrows) (right panels). **(C)** Expression of MMPs (MMP2, n=6; MMP9, n=3), membrane-type MMPs (n=3), and their corresponding tissue MMP inhibitors, TIMP1 (n=3)

and TIMP2 (n=6), mRNA was significantly increased in the *Neu1*$^{-/-}$ *gastrocnemius* muscle. * = p<0.05, ** = p<0.01; *** = p<0.001; Student's t test.

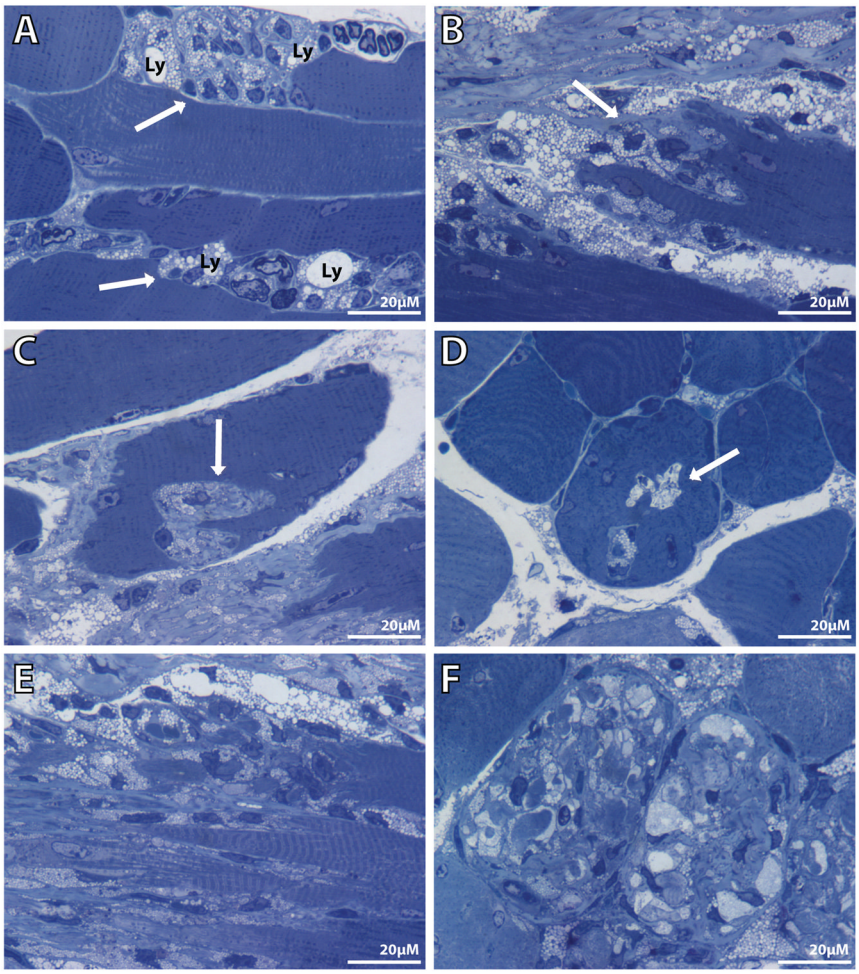

Fig. 6.

Toluidine blue–stained semi-thin *Neu1*$^{-/-}$ *gastrocnemius* muscle sections show different stages of connective tissue infiltration and muscle fiber invagination. **(A)** Enlarged lysosomes (Ly) are observed in the cytosol of proliferating fibroblast-like cells (arrows) at the endomysium space in a longitudinal section. **(B and C)** Invagination of the sarcolemma with infiltration of the muscle fibers by ECM components (arrows). **(D)** This invagination extends the length of the myofiber and appears as vacuole-like structures (arrow) in the transverse view. In a more advanced stage, ECM invagination has resulted in severe fragmentation of the cytosol and complete disruption of the muscle cytoarchitecture in **(E)** longitudinal and **(F)** transverse sections.

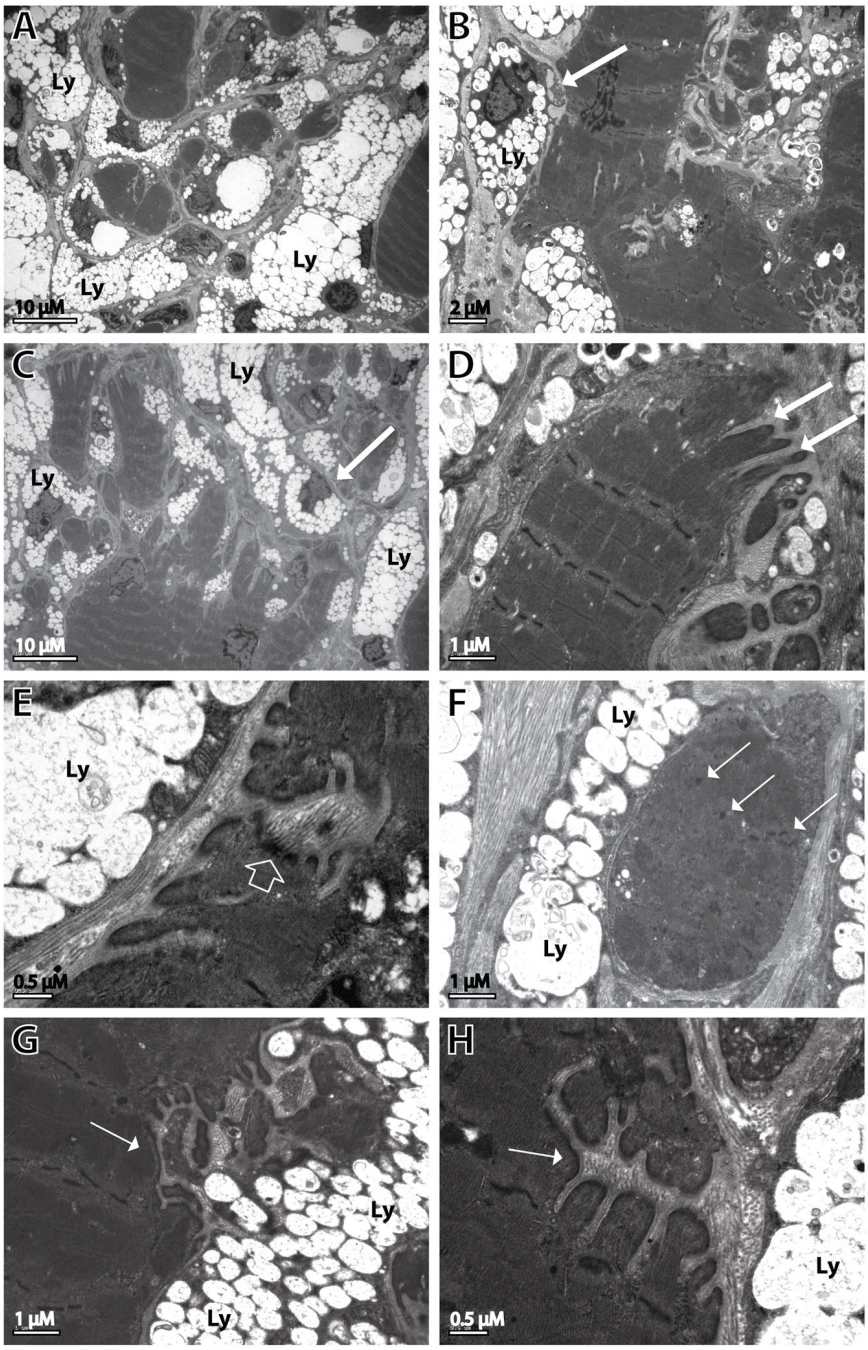

Fig. 7.

Ultrastructural analysis of *Neu1*$^{-/-}$ *gastrocnemius* muscle. The EM images reveal fibers showing the fragmentation of the cytosol, sarcolemmal changes, and disorganization of the internal cytoarchitecture. **(A-C)** Cytosolic fragmentation and infiltration of muscle fibers by fibroblast-like cells (arrows) whose cytosol is filled with storage lysosomes (Ly). **(D, G and H)** Digit-like invaginations (arrows) and **(E)** thickening of the sarcolemma (open arrow). **(F)** Cytosolic fragments within an individual muscle fiber with disorganization of the internal architecture and Z-line aggregates (arrows).

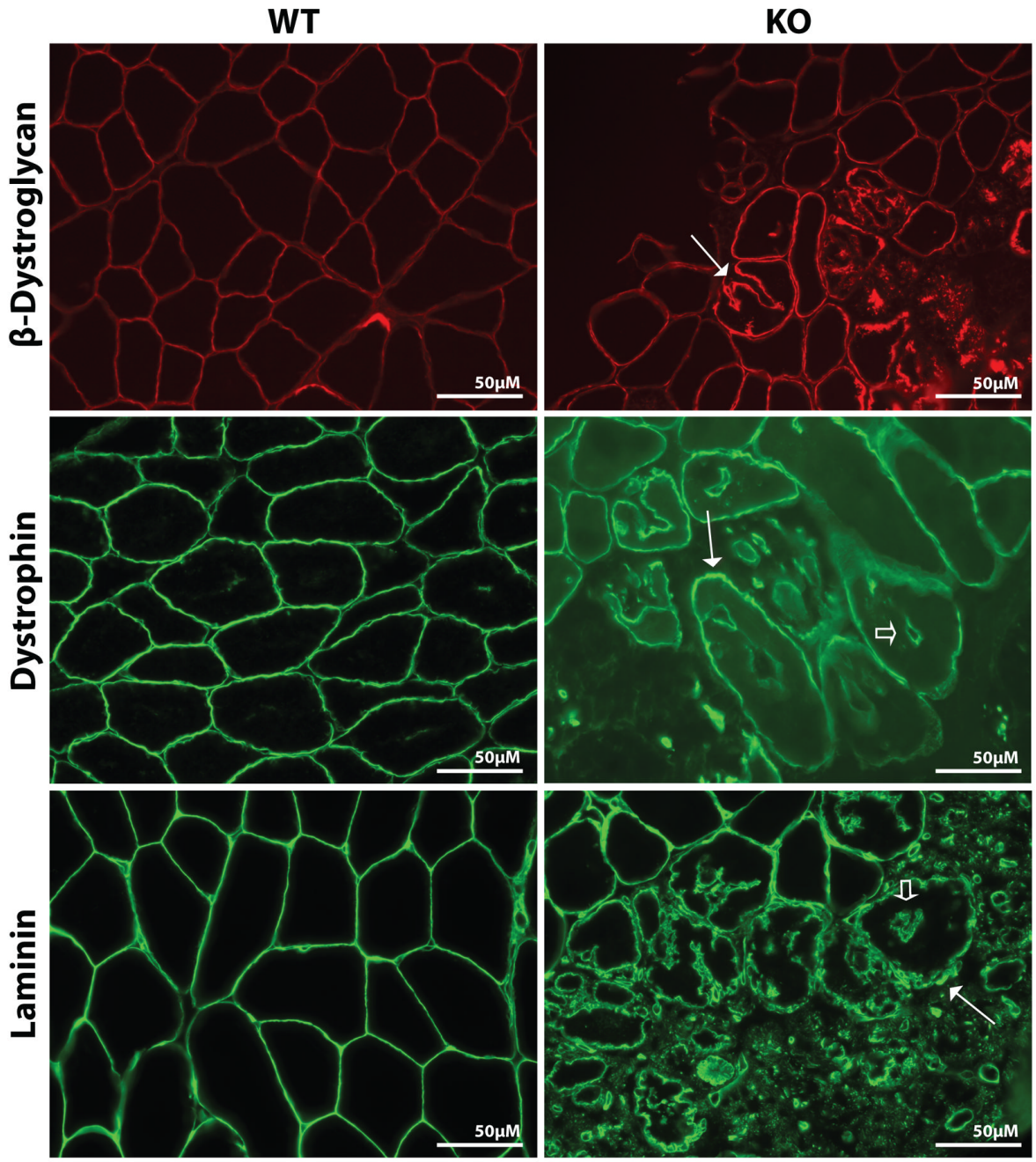

Fig. 8.

Immunofluorescence staining of transverse *Neu1*$^{-/-}$ (KO) *gastrocnemius* muscle. Sections for sarcolemmal proteins β-dystroglycan (red), dystrophin (green) and basal laminal protein laminin (green) show intense fragmentation with destruction of the myofibers next to the perimysium. The expression of these proteins is higher in the sarcolemma of the affected muscle fibers (arrows) than in WT tissue. The vacuole-like structures stained positive for dystrophin and laminin (open arrows).

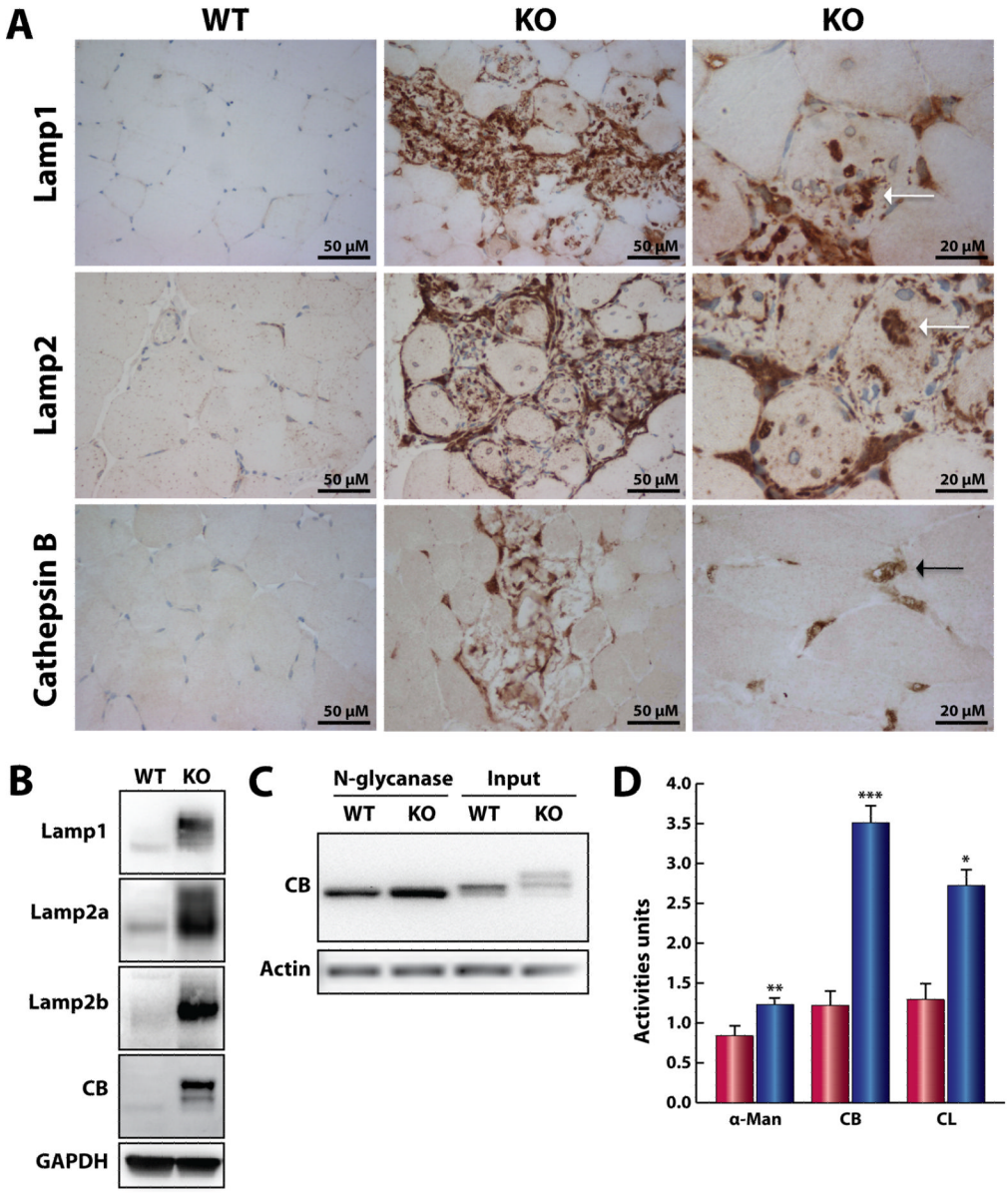

Fig. 9.

Accumulation of lysosomal components in the ECM of *Neu1*$^{-/-}$ (KO) skeletal muscle. **(A)** Increased Lamp-1, Lamp-2, and cathepsin B protein expression in the infiltrated areas and within the infiltrated muscle fibers (white arrows) of *Neu1*$^{-/-}$ muscle. Cathepsin B protein expression was also increased in the cells located in the endomysium space (black arrow) (bottom right panel). **(B)** Lamp-1, Lamp-2a, Lamp-2b, and cathepsin B protein expression was increased and showed different mobility patterns on SDS-PAGE gel of *Neu1*$^{-/-}$ *gastrocnemius* muscle lysates. **(C)** Deglycosylation of cathepsin B by N-glycanase. **(D)** The activity of α-mannosidase (αman) and cathepsins B (CB) and L (CL) in the culture medium collected from *Neu1*$^{-/-}$ fibroblasts (blue bars, n=3) was also higher than that from WT cells (red bars, n=3). * = $p<0.05$, ** = $p<0.01$; *** = $p<0.001$; Student's t test.